

Mechanical Design of Fiber-Wound Hydraulic Skeletons: The Stiffening and Straightening of Embryonic Notochords¹

M. A. R. KOEHL,^{2,*} KIM J. QUILLIN,^{*} AND CHARLES A. PELL[†]

^{*}*Department of Integrative Biology, University of California, Berkeley, California 94720-3140*

[†]*Nekton Technologies, Inc., 710 Main St., Durham, North Carolina 27701*

SYNOPSIS. The notochord can play an important mechanical role in shape changes during early morphogenesis of vertebrates. For example, osmotic inflation of notochords elongates and straightens the axis of frog early tail-bud embryos. In *Xenopus laevis*, the sheath of cross-helically arranged fibers around the notochord limits the shape changes it undergoes when inflating, causing the notochord to stiffen and straighten (Adams *et al.*, 1990; Koehl *et al.*, 1990). We used physical models of stage 24 *X. laevis* notochords to explore the mechanical consequences of different arrangements of the sheath fibers on the behavior of such curved hydraulic cylinders. All the models straightened upon inflation regardless of initial fiber angle (θ = angle of the fibers to long axis of the cylinder). Notochord models with $\theta > 54^\circ$ lengthened and narrowed as they straightened; although they could push, the forces they exerted were limited by their tendency to buckle, which increased the greater the θ . In contrast, models with $\theta < 54^\circ$ shortened and widened as they straightened and showed pronounced increases in flexural stiffness. The mean θ of *X. laevis* early tail-bud notochords is 54° , a fiber angle that permits an increase in the end-to-end distance of the model (along the anterior-posterior axis of the embryo) as it straightens and pushes when pressurized, but that is less prone to Euler and local buckling than are models with higher θ 's. Nonetheless, a θ of 54° in notochords may simply be the result of osmotic swelling.

INTRODUCTION

The notochord plays a variety of important inductive and mechanical roles in the development of vertebrate embryos (reviewed in Adams *et al.*, 1990; Koehl *et al.*, 1990; Gilbert, 1985). One of its early mechanical functions is to elongate and straighten the anterior-posterior axis of the embryo between the late neurula and early tailbud stages. A number of studies of amphibian or chick embryos have shown that removal or disruption of the notochord by a variety of techniques greatly reduces the elongation of embryos during these stages (reviewed in Adams *et al.*, 1990).

We studied the biomechanics of the elongation and straightening of the notochord of early frog embryos, focusing on *Xenopus laevis* embryos at stages 21 (late neurula) to 28 (early tailbud) (Adams *et al.*, 1990;

Koehl *et al.*, 1990) (Fig. 1). The notochord is composed of a stack of flat cells surrounded by a connective tissue sheath. The density of the collagen fibers in the sheath increases and the osmotic activity of the vacuoles in the notochord cells rises during these stages. The swelling of the vacuoles is resisted by the sheath, so the internal pressure of the notochord rises 2- to 3-fold. The notochord elongates and straightens and its flexural stiffness increases by an order of magnitude during these stages of development. Removal of the sheath by collagenase digestion drastically reduces the flexural stiffness of the notochord. Such a floppy, sheathless notochord cannot push effectively on the surrounding embryonic tissues, but rather folds up like a wet noodle as it elongates relative to the surrounding embryo (Fig. 5 in Koehl *et al.*, 1990). Thus, the early amphibian notochord is a hydraulic skeleton that uses osmotic inflation as a mechanism of force-generation and shape-change production, and the fibrous sheath is essential for its mechanical function. We found that the fibers in the sheath of *X. lae-*

¹ From the symposium *The Function and Evolution of the Vertebrate Axis* presented at the Annual Meeting of the Society for Integrative and Comparative Biology, 6–10 January 1999, at Denver, Colorado.

² E-mail: cnidaria@socrates.berkeley.edu

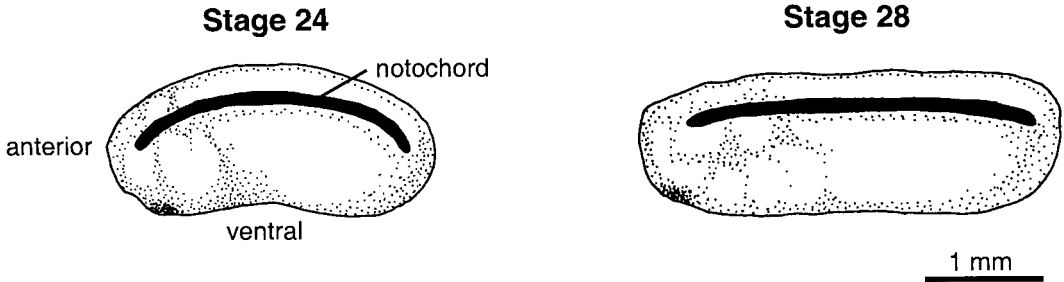


FIG. 1. Profiles of *Xenopus laevis* embryos at two stages of development (24 and 28 hr after fertilization at 22°C), indicating the straightening and elongation of the notochord and the embryo (drawn from data and SEMs presented in Adams *et al.*, 1990, and Koehl *et al.*, 1990).

vis notochord during these stages of development are oriented at a mean angle of 54° with respect to the long axis of the notochord.

Hydraulic skeletons

A hydraulic skeleton is composed of a tension-resisting container inflated by compression-resisting fluid under pressure. The function of such skeletons, as well as many examples of their occurrence in the Plant and Animal Kingdoms, are reviewed by *e.g.*, Chapman (1958, 1975), Clark (1964), Green (1980), Cosgrove (1987), and Wainwright (1988). Some of these hydraulic skeletons, such as notochords (*e.g.*, Adams *et al.*, 1990; Koehl *et al.*, 1990; Koob *et al.*, 1994; Fennaux, 1998) and plant cells (*e.g.*, Green, 1980; Cosgrove, 1987) are inflated osmotically, whereas others, such as echinoderm tube feet (*e.g.*, Woodley, 1967) and mammalian penises (*e.g.*, Kelly, 1997), are inflated by muscle contractions elsewhere in the body that force fluid into the container. Most biological hydraulic skeletons are cylindrical and their walls are reinforced by relatively inextensible fibers (usually collagen or chitin in animals, and cellulose in plants). The shape changes that such hydraulic systems undergo when inflated are constrained by the orientation of the fibers reinforcing their walls (*e.g.*, Clark and Cowey, 1958; Clark 1964). Fiber orientation is expressed as fiber angle (θ), the angle between the fibers and the long axis of the cylinder.

Mathematical models have been developed for various pressurized, fiber-reinforced cylindrical systems (*e.g.*, plant cells,

worms, echinoderm tube feet, whales, man-made pressure vessels and hydraulic actuators) to predict the shape changes that occur when these structures are inflated, subjected to external loads, or deformed by contractions of muscles in their walls (*e.g.*, Sherrer, 1967; Swanson, 1974; Hettiaratchi and O'Callaghan, 1978; Woodley, 1980; Alexander, 1987; Wadepuhl and Beyn, 1989; Tondu and Lopez, 1995; Chou and Hannaford, 1996; Skierczynski *et al.*, 1996), but none of these address the issue of the forces exerted by inflating, curved, fiber-reinforced hydraulic systems like the embryonic notochord. A few measurements have been made of the flexural stiffness of various hydraulic cylinders in animals, such as the notochords of frog embryos (Adams *et al.*, 1990; Koehl *et al.*, 1990) and sturgeon adults (Long 1995), and of artificially-inflated armadillo penises (Kelly, 1999).

Objectives of this study

The purpose of this study was to investigate how the orientation (θ) of the reinforcing fibers in the walls of curved hydraulic cylinders, such as the notochords of early tail-bud frog embryos, affects their mechanical performance when they are inflated. If an inflating notochord is to straighten and elongate the embryo, it must straighten when pressurized and the distance between its anterior and posterior ends must increase. When undergoing these shape changes, it must be stiff enough to exert forces and do work along the anterior-posterior axis of the embryo without bowing or kinking. Therefore, the specific aspects of performance that we studied were:

1) shape changes when inflated, 2) resistance to bending (flexural stiffness), 3) axial forces exerted and work done when inflated, 4) resistance to elastic bowing (Euler buckling), and 5) resistance to kinking (local buckling).

MATERIALS AND METHODS

Fabrication of models

We used physical models of fiber-reinforced curved hydraulic cylinders to study the consequences of fiber angle (θ) on mechanical performance. Models offered several advantages over real notochords to address this issue. By using models, we were able to vary just the parameter of interest, θ , while holding constant the shape and the materials (fibers and matrix) from which the walls were constructed. We could control the internal pressure and measure defined aspects of the mechanical performance of the models. Not only could we hold all parameters constant except the one we wanted to test, but we could also test θ 's not available in nature. Furthermore, since stress similarity is maintained in hydrostatic cylinders of different sizes if they are geometrically similar (Quillin, 1998), we could use large models to assess the design of tiny notochords. While the measurement of forces and mechanical properties of parts of microscopic embryos is technically challenging (*e.g.*, Adams *et al.*, 1990; Koehl *et al.*, 1990; Koehl, 1990; Moore *et al.*, 1995), measurements of mechanical performance of large models is much easier.

Our purpose in using models was to explore the *relative* performance of curved hydraulic cylinders reinforced with inextensible fibers at different θ 's. Since we were not trying to predict exact shape changes, forces, work, or buckling by real notochords in embryos, we did not attempt to model the tissues that surround the notochord *in vivo*, nor did we try to measure the tensile elastic modulus (E , resistance to stretching, see Wainwright *et al.*, 1976) of real notochord sheath in order to replicate that E in our fabricated sheaths.

We used morphometric data (Adams *et al.*, 1990) to design physical models that

were geometrically similar to the notochords of *Xenopus laevis* embryos at stage 24. We chose stage 24 because the significant increases in internal pressure and flexural stiffness of the notochord occur just after this stage of development in *X. laevis* (Adams *et al.*, 1990; Koehl *et al.*, 1990). The notochord sheath is a collagenous connective tissue (evidence reviewed in Adams *et al.*, 1990). Since collagen fibers in such tissues are relatively inextensible while the proteoglycan matrix around them is deformable (*e.g.*, Wainwright *et al.*, 1976), we modeled the collagen by using relatively inextensible nylon fibers (organza fabric) and the matrix by using compliant polyurethane (Skinflex III castable polyurethane, BJB Enterprises). Neither water nor air leaked through the polyurethane matrix, hence we could inflate the models.

We fabricated the models by the following process. The sheath of fibers was made by sewing into a tube a strip of organza cut on the bias. The warp and woof fibers of the organza, which were of the same diameter, thus formed right- and left-handed helices around the tube. The weave of the fabric was loose enough that the angle between the warp and woof fibers could be easily manipulated to mimic crossed-helical arrays of different θ 's. Black lines were drawn along warp and woof fibers at 2 to 5 cm intervals so that the orientations of the fibers could be easily seen on completed models. Cylinders of organza were sewn (zig-zag stitch to permit easy deformation of the seam) such that they assumed the desired fiber angle when fitted over a mandrel (Murphy, 1990) that was geometrically similar to the curved notochord of a stage-24 *X. laevis* embryo. The mandrel was coated with a layer of latex that was allowed to polymerize while the mandrel was rotated about its long axis by a motor to maintain an even distribution of polyurethane. The organza sheath was then slipped over the mandrel and impregnated with another coating of polyurethane, and the mandrel was again rotated while the polyurethane polymerized. Three replicate models were made of each of the following fiber angles: 34°, 45°, 54° (to mimic *X. laevis* notochords), and 63°.

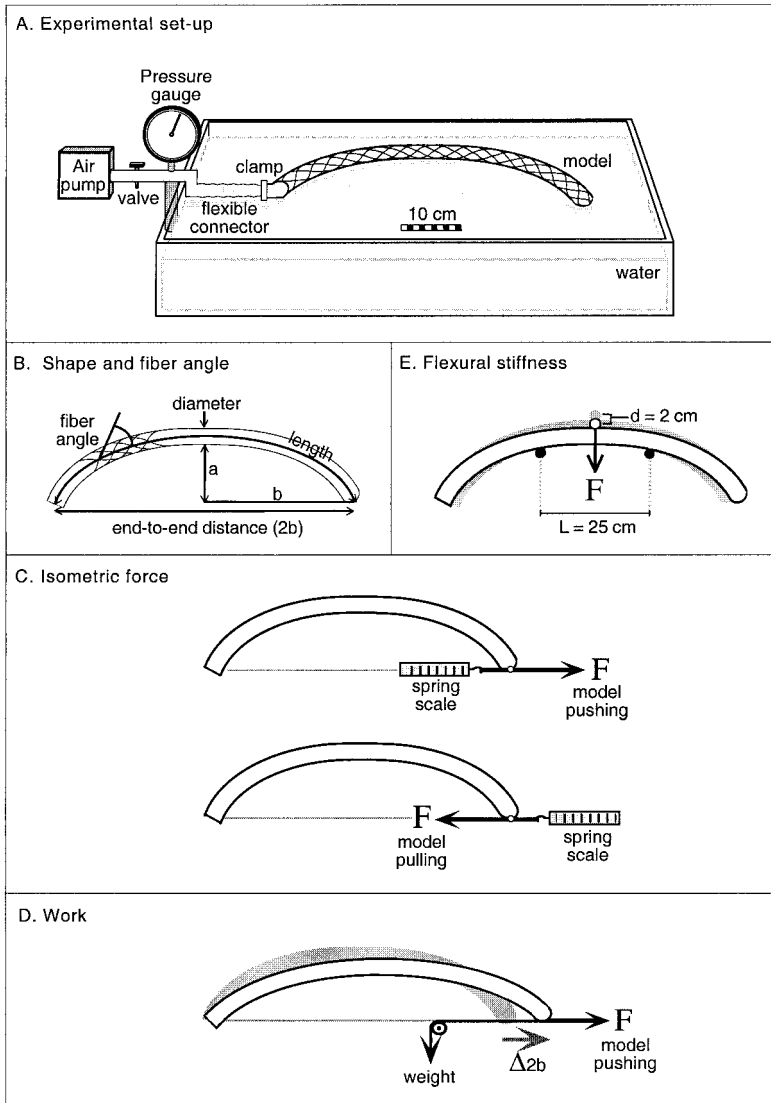


FIG. 2. Schematic summary of experiments conducted on model notochords. The experimental set-up shown in A was used for all measurements (B–E). The details of the experimental protocols illustrated in B–E are given in Materials and Methods. Note that only some of the fibers are drawn in these diagrams of the models; the organza fabric used to construct the models had 36 warp and 36 woof fibers per cm^2 .

Inflation and measurement of internal pressure

Our experimental set-up is diagrammed in Figure 2A. To avoid effects of friction or gravity on the behavior of the models, we inflated the models with air and we floated them on the surface of a water bath. Each model was clamped to a flexible pipe in series with a pressure gauge (Omega PGS-

35L–60; 60 psi full scale = 414 kN/m^2), a two-way-valve, and a manual air pump (bicycle pump). After inflating the models to the target pressures of 14, 28, 41, and 55 kN/m^2 ($\pm 2 \text{ kN/m}^2$), we closed the valve to maintain constant pressure during measurements. We did not use pressures above 55 kN/m^2 so that we could prevent rupture of the models. The flexible connector enabled

us to reposition the models on the water surface to prevent the models from touching the walls of the water bath after shape changes. All measurements were made at room temperature (24°C).

Measurement of size, shape and fiber angle

Changes in shape and fiber angle were measured using photographic images of each of the twelve models inflated to 0, 14, 28, 41, and 55 kN/m². We used a 35 mm camera mounted above the water tank (camera lens parallel to the surface of the water bath) to photograph the models. We then projected the images of the models with a slide projector onto a Jandel Scientific digitizing tablet (San Rafael, California 94901). Model length, diameter, fiber angle, end-to-end distance, and curvature (Fig. 2B) were digitized from the projected images using Sigma Scan software (version 3.9). A scale bar in each image provided the reference points for calibrating the measurements on each model. The length of the midline of a model was calculated as the mean of six measurements: three measurements of the outside length (convex side) and three measurements of the inside length (concave side) of the model. Lengths were measured to the nearest 1 mm. The diameter of a model was calculated as the mean of three measurements of the diameter at the midpoint of the model. Diameter was measured to the nearest 0.1 mm. Measurements of the angle between fibers that crossed each other near the midline of a model were made at twenty positions distributed along the length of each model; each mean angle was multiplied by 0.5 to yield θ , the angle between the fibers and the long axis of the model. Fiber angle was measured to the nearest 1 degree. The end-to-end distance (2b in Fig. 2B) from the tip to the base of the model was calculated as the mean of three measurements to the nearest 1 mm. The distance (a, Fig. 2B) between the midpoint of 2b and the midpoint of the model (perpendicular to 2b) was also calculated as the mean of three measurements to the nearest 0.1 mm. Curvature was then calculated as a/b (Fig. 2B).

To estimate the inside volume of the in-

flated models, it was necessary to first measure the wall thickness of the models. We measured wall thickness directly using electronic calipers. The double thickness of each flattened, intact model was measured to the nearest 0.1 mm at the midpoint and half way between the midpoint and each end. The three values were summed and divided by six to derive a mean wall thickness for each model. Variation in model wall thickness was due to variation in thickness of the latex matrix, not due to variation in thickness of the fiber sheath. To estimate internal volume, wall thickness was assumed not to change as the models were inflated. (Because inflated models that lengthened also became narrower, while those that shortened became wider, wall thickness changed very little during inflation. The calculated maximum change in wall thickness during inflation for the models was smaller than the standard deviation of our measurements of thickness.) Model volume was then calculated by the equation:

$$V = \pi L(D/2 - t)^2 \quad (1)$$

where V is the internal volume, $\pi = 3.14$, L is the midline length at a given pressure, D is the midpoint diameter at a given pressure, and t is the wall thickness.

Measurement of isometric forces

When the notochord models were inflated, their lengths, diameters, end-to-end distances, and curvatures were subject to change. For the measurements of isometric force, we held the end-to-end distance constant (Fig. 2C). No constraints were used to limit shape changes other than end-to-end distance in pulling models ($\theta < 54^\circ$; where midline length decreased, and hence curvature decreased). However, since the midline length of pushing models ($\theta > 54^\circ$) increased during inflation, such models tended to bow out laterally (Euler buckling) or kink (local buckling) when the distal end of the model was restrained to maintain a fixed end-to-end distance. Therefore, such models were tested in a curved wooden trough. Each model was placed in the trough, which was the shape of an uninflated model, and a clear plexiglas lid was placed over

the trough. As each model was inflated, the walls of the trough prevented the curved notochord model from buckling dorso-ventrally (see Fig. 1), while the floor and lid of the trough prevented it from buckling laterally. The trough, which was 4 mm wider than the models, had a square cross-section to minimize contact area with models, which had circular cross-sections. Effects of friction between the smooth interior of the trough and the models on force measurements were minimized by lubricating the model and the trough with a liberal coating of latex-safe lubricant (K-Y Jelly, Johnson and Johnson). However, the isometric force may have been slightly underestimated due to pushing by the models on the trough walls.

As each model was inflated to 14, 28, 41, and 55 kN/m², we measured the force required to prevent the end-to-end distance from shortening or elongating. Both pulling and pushing forces were measured using a hand-held spring scale attached to the end of the model and oriented along the end-to-end axis (Fig. 2D). An Ametek spring scale (Trim series; 50 N full scale) was used for models that pulled (attempting to decrease the end-to-end distance) and force was measured to the nearest 0.5 N. A Homs spring scale (Model 2; 10 N full scale) was used for models that pushed (attempting to increase the end-to-end distance) and force was measured to the nearest 0.05 N. Since spring scales operate by elongating under loads, it was necessary to adjust the position of the spring scale as the models exerted force such that the end-to-end distance was maintained during inflation. The forces at all four pressures were measured three times for each of the three models for each fiber angle.

Measurement of work

In order to elongate the embryo, the notochord must do work on the surrounding tissues as it straightens. We determined how much pushing work could be done by the models for given increments in internal pressure as the end-to-end distance (corresponding to the anterior-posterior axis of the embryo) was allowed to change. To achieve this, we applied known weights to

the tip of the models using pulleys so that the weights compressed the models along the end-to-end axis (Fig. 2D). The end-to-end distance was then measured with a ruler to the nearest 0.5 cm after the models were inflated to pressures of 14, 28, 41, and 55 kN/m². Since the models changed shape as they were inflated, the clamped bases of the models were rotated when necessary to maintain the pull of the weight along the end-to-end axis. First we used a weight that approximated the maximum weight that a model of a given fiber angle could sustain without buckling. We then chose three other smaller weights to provide an evenly-distributed range of loads for each model.

Work was calculated as the pushing force (equal in magnitude and opposite in direction to the weight tending to decrease the end-to-end distance of the model) times the distance that the force moved (the increase in end-to-end distance that occurred when the pressure was increased). Work was thus determined three times for each model subjected to each weight, and the mean was calculated. We defined positive work as work that increased the end-to-end distance of the models (corresponding to work by a notochord that would push along the anterior-posterior axis of the embryo and elongate it). Since we measured the end-to-end distance at each pressure, the change in this distance during an increase in internal pressure was calculated by taking the difference in the two end-to-end distances for each consecutive pair of pressures. Note that the 34° and 45° models shortened upon inflation when not bearing a load; when subjected to a compressive load, they bent and their end-to-end distances were shorter still. However, when such models bearing compressive loads were then inflated to a higher pressure while bearing a load, they straightened and their end-to-end distances increased against the load, and thus they did pushing work. As a result, models of all fiber angles were able to do positive pushing work.

Measurement of flexural stiffness

Flexural stiffness is a measure of the resistance of a unit length of column or beam to being bent (*e.g.*, Wainwright *et al.*, 1976). We used a standard three-point

bending apparatus (Fig. 2E) to measure the flexural stiffness of model notochords at different pressures (14, 28, 41, and 55 kN/m²), treating the notochord as a simply-supported beam subjected to a point load at its center. The end-supports of the three-point bending apparatus consisted of two wooden dowels anchored 25 cm apart, perpendicular to the surface of the water bath. The models were loaded at the center by a third dowel that was pulled laterally by a line which was in turn threaded through a series of three pulleys at the edge of the water bath and connected to a basket of calibration weights hung over the side of the water bath. We applied weights incrementally until the lateral deflection of the models was 2 cm (measured to the nearest 1 mm using a ruler), which was a small deflection (less than 10% of the 25 cm distance between supports). The total load of calibration weights plus basket applied was measured to the nearest gram.

We calculated flexural stiffness (S_{flex}) using the following expression for beams subjected to small deflections in three-point bending:

$$S_{\text{flex}} = FL^3/48\delta \quad (2)$$

where F is the force, L is the length of the beam between the two supports, and δ is the lateral deflection of the beam (Wainwright *et al.*, 1976). Flexural stiffness was thus determined three times for each model and the mean was calculated.

Calculation of critical force to cause Euler buckling

A column bearing a compressive load can undergo Euler buckling (*i.e.*, elastic bowing) if the load exceeds a critical force. Flexural stiffness (S_{flex}) was used to calculate how much force would be required to cause Euler buckling of each model. Because the models became straight when inflated to the highest internal pressure we used in our experiments (55 kN/m²), we calculated the critical force to cause Euler buckling for models at that pressure using the equation for a straight column with un-fixed ends:

$$F_{\text{crit}} = \pi^2(S_{\text{flex}})/L_c^2 \quad (3)$$

where L_c is the length of the column (Wainwright *et al.*, 1976). F_{crit} was thus determined three times for each model and the mean was calculated. This F_{crit} was used simply as an index of the resistance to Euler buckling so that we could compare the *relative* performance of hydraulic cylinders wrapped with fibers at different θ 's. Real notochords might be less likely to undergo bowing since they are surrounded by other tissues. On the other hand, curved columns (such as notochords in stage 24 embryos of *X. laevis*) should be more susceptible to Euler buckling than are relatively straight ones such as notochords of stage 28 *X. laevis* embryos or our fully-inflated models.

Calculation of index of resistance to kinking

A hollow cylindrical column bearing a compressive load can fail by local buckling (kinking like a soda can). The critical local compressive stress (σ_{crit}) that produces a kink in the wall of such a cylinder is given by

$$\sigma_{\text{crit}} = kEt/(2r) \quad (4)$$

where E is the elastic modulus (resistance to deformation) of the material from which the cylinder is made, t is the thickness of the wall of the cylinder, r is the cylinder's outside radius, and k is a constant that depends on how the ends of the column are anchored (*e.g.*, Wainwright *et al.*, 1976). Hence, lower stresses are required to kink wide tubes than to kink slender ones.

Whether or not a column kinks when loaded depends on the magnitude of the compressive stresses it experiences relative to its σ_{crit} . If a column or beam is subjected to a load that tends to bend it, then the maximum compressive stress in its wall (σ_{max}) is given by

$$\sigma_{\text{max}} = Mr/I \quad (5)$$

where r is the outside radius, I is the second moment of area, and M is the moment loading the column or beam (for example, in the simple case of a cantilevered beam bent by a point load (F) at its end, $M = F L_c$, where L_c is the length of the beam) (Wainwright *et al.*, 1976). The I of a hollow cylindrical column or beam is given by

$$I = [\pi r^4 - \pi(r - t)^4]/4 \quad (6)$$

where t is wall thickness and r is radius (Alexander, 1983). Thus, for a given load tending to bend a column or beam, stresses are much greater in long, slender ones than in short, wide ones.

A cylinder containing a pressurized fluid is more resistant to kinking than an unpressurized hollow cylinder because the stretching of the cylinder walls by the internal pressure counteracts the compression of the walls by bending loads. The maximum net compressive stress (σ_{net}) in the wall of a pressurized cylinder subjected to a load that tends to bend it is thus

$$\sigma_{\text{net}} = \sigma_{\text{max}} - \sigma_{\text{press}} \quad (7)$$

where σ_{press} is the longitudinal tensile stress in the wall of a cylinder containing a fluid under pressure; σ_{press} is given by

$$\sigma_{\text{press}} = Pr/(2t) \quad (8)$$

where P is the internal pressure, r is the outside radius, and t is the wall thickness (Wainwright *et al.*, 1976). The wider a pressurized cylinder of a given wall thickness, the greater its σ_{press} for a given internal pressure.

A rough index of the susceptibility of a pressurized cylinder to local buckling is the ratio of σ_{crit} to σ_{net} , which we calculated using equations (4) through (8). We calculated this index for a load of 1 N. The elastic modulus (E) of the nylon-latex composite walls of our models was of order 10^8 N/m² (Koehl and Quillin, unpublished data), the internal pressures (P) used in our experiments were of order 10^4 N/m², and k is of order 1 (Wainwright *et al.*, 1976). We used these approximate values to calculate $\sigma_{\text{crit}}/\sigma_{\text{net}}$ for every model because this ratio was meant to be a simple index of the *relative* resistance to kinking of cylinders reinforced with fibers at different angles (if the cylinders are made of the same material, have the same internal pressure, and are loaded in the same manner by a given force). The ratio of σ_{crit} to σ_{net} was thus determined for each model.

Calculations and statistical analyses

Data were entered into spreadsheets and the calculations described above as well as

statistical analyses were done using Microsoft Excel 98 software. Each parameter was measured or calculated for three separate measurements for each model, and a mean was determined for that model. Three replicate models were tested for each fiber angle, so the mean value of a parameter from each model was used to calculate the overall mean and the 95% confidence intervals for models of a given θ . The only exception to this was the index of resistance to kinking, for which one value was calculated for each model using the mean values for that model of the relevant parameters; the mean of this index for the three replicate models of each fiber angle was then calculated. The overall means for models of different θ were taken to be significantly different from each other if their 95% confidence intervals did not overlap.

RESULTS

Shape changes during inflation

The fiber angle, θ , of the models determined the shape changes they underwent when inflated. Cylinders with fiber angles $>54^\circ$ became longer and slimmer, while those with fiber angles $<54^\circ$ became shorter and wider when inflated (Fig. 3), as had been predicted by geometrical calculations (Clark and Cowey, 1958). The fiber angles of all the models converged towards $\sim 55^\circ$ as they were inflated (Fig. 4); $54^\circ 44'$ is the θ at which the maximum volume can be contained in a cylinder wound with inextensible fibers (Clark and Cowey, 1958). When models whose initial fiber angle was 54° were inflated, they did not change measurably in length, diameter, or θ .

All the curved models straightened upon inflation, regardless of initial fiber angle (Fig. 5A). As the models wound with fibers at 63° or at 54° were inflated and became less curved, the distance between the two ends of the cylinder (2b; see Fig. 2B) increased. In contrast, when models with θ 's of 34° and 45° were inflated, their end-to-end distance (2b) decreased as they straightened (Fig. 5B). The change in end-to-end distance produced by a given increase in the volume of an inflating cylinder was greater for the models wound at high

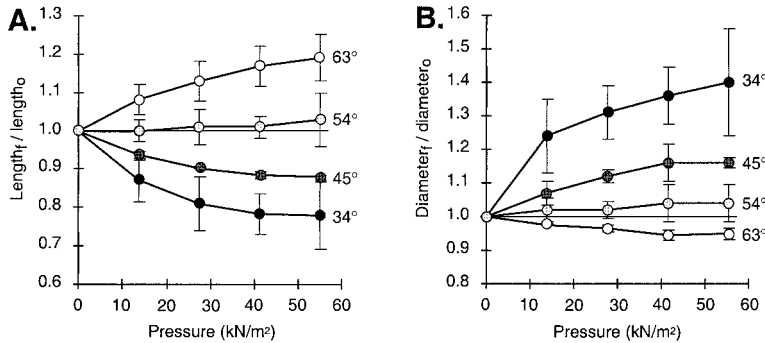


FIG. 3. Dimensions of model notochords during inflation. Each line represents the values for models reinforced with fibers at the θ indicated to the right of the line. Each symbol represents the mean of the mean values from three replicate models. Error bars represent 95% confidence intervals. A. Model length (Fig. 2B) when inflated (Length_t) normalized to model length when uninflated (Length_0), plotted as a function of the pressure in the model. Values of ($\text{Length}_t/\text{Length}_0$) greater than 1 indicate lengthening, while those lower than 1 indicate shortening. B. Model diameter (Fig. 2B) when inflated (Diameter_t) normalized to model diameter when uninflated (Diameter_0), plotted as a function of the pressure in the model. Values of ($\text{Diameter}_t/\text{Diameter}_0$) greater than one indicate widening, while those lower than one indicate narrowing.

fiber angles than it was for those wound at low angles (Fig. 6).

Mechanical performance

Flexural stiffness. The resistance to bending (flexural stiffness) of all the models increased as they were inflated and their internal pressure increased. However, this stiffening effect was less pronounced for models with high θ 's that became long and slender upon inflation than it was for those with low θ 's that became short and wide when pressurized (Fig. 7A). Therefore, the

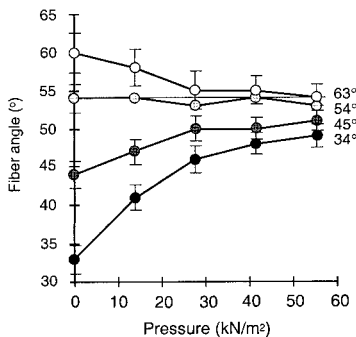


FIG. 4. Fiber angles of model notochords during inflation, plotted as a function of the pressure inside the model. Each line represents the values for models that, when uninflated, had fibers at the θ indicated to the right of the line. Each symbol represents the mean of the mean values from three replicate models. Error bars represent 95% confidence intervals.

higher the initial fiber angle, the lower the flexural stiffness for a given internal pressure.

Isometric force and work. When the models were inflated, they could exert force and do work. We focused on the forces exerted and work done along the end-to-end axis of the models (Fig. 2C and D) that corresponded to the anterior-posterior axis of the embryo (Fig. 1). Models reinforced with high θ 's pushed when inflated, while those with fibers at low θ 's pulled. The isometric forces produced by the models reinforced with fibers near 54° were very sensitive to fiber angle: the models with mean θ 's slightly below $54^\circ 44'$ (53° and 52°) pulled, while the model with a mean θ slightly above $54^\circ 44'$ (57°) pushed. For a given internal pressure, the isometric pushing forces exerted by models with θ 's of 63° were greater than those exerted by models with θ 's of 54° (Fig. 7B), while the isometric pulling forces exerted by models with θ 's of 34° were greater than those produced by models with θ 's of 45° (Fig. 7B).

If the pressure was increased in a model while it was bearing a compressive load, it could push against that load and do work in the direction that would elongate the axis of the embryo (Fig. 2D). This was true not only for models with high θ 's that elongated when inflated (63° and 54°), but also for

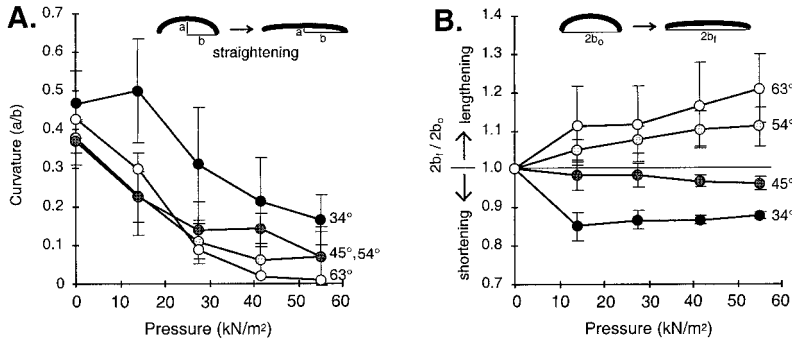


FIG. 5. Shape changes of models during inflation. Each line represents the values for models reinforced with fibers at the θ indicated to the right of the line. Each symbol represents the mean of the mean values from three replicate models. Error bars represent 95% confidence intervals. A. Curvature (a/b) of model notochords plotted as a function of the pressure inside the model. B. End-to-end distance (along the axis corresponding to an embryo's anterior-posterior axis) of model notochords during inflation, plotted as a function of the pressure inside the model. End-to-end distance when inflated ($2b_1$) was normalized to end-to-end distance ($2b_0$) when uninflated. Values of $2b_1/2b_0$ greater than one indicate elongation of the end-to-end axis, while values less than one indicate shortening of that axis.

models with low θ 's that shortened (45° and 34°). Even though there was a fair bit of scatter in the data, they indicated that, for a given load, models with higher θ 's could do more pushing work along the axis that corresponded to the anterior-posterior axis of an embryo than could models with low θ 's (Fig. 7C). However, there was a limit to the magnitude of the load against which a model could work: if the load was too high, the

model buckled and could not push the load. Therefore, although models with high θ 's could do more work against a given load, models with low θ 's could work against higher loads without buckling (Fig. 7C).

Euler buckling and local buckling. A column pushed on its ends can undergo Euler buckling (elastic bowing) or can undergo local buckling (kinking). Models with high θ 's that became long and slender when inflated were more likely to undergo Euler buckling when loaded like a column than were models with low θ 's that became short and wide and had higher flexural stiffnesses (Fig. 8A). Similarly, for a given internal pressure, models with high θ 's were less resistant to kinking than were those with low θ 's (Fig. 8B). Even though higher stresses are required to kink slender tubes than wide ones ($\sigma_{\text{crit}} \propto 1/r$), the net compressive stress (σ_{net}) experienced by long, slender tubes is higher than for short, wide ones bearing the same compressive or bending load. This is because: 1) the tensile stresses (σ_{press}) caused by a given internal pressure that counteract kinking are greater in the walls of wide cylinders than of slim ones ($\sigma_{\text{press}} \propto r$), and 2) the compressive stresses tending to produce a local buckle are greater in long, slender tubes than in short wide ones subjected to the same bending load ($\sigma_{\text{max}} \propto L_c/[r^3]$).

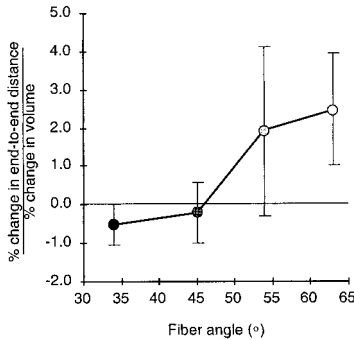


FIG. 6. Percent end-to-end elongation of notochord models per percent increase in volume when models were inflated to an internal pressure of 14 kN/m^2 , plotted as a function of the fiber angle of the model when uninflated. Negative values of $[(\% \text{ change in end-to-end distance})/(\% \text{ change in volume})]$ indicate that the models shortened along the end-to-end axis when inflated, while positive values indicate that the models elongated along that axis. Each symbol represents the mean of the mean values from three replicate models. Error bars represent 95% confidence intervals.

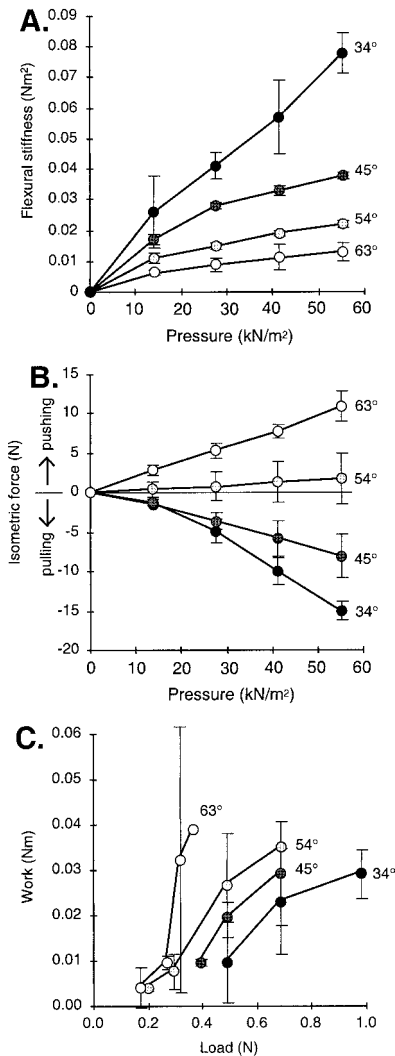


FIG. 7. Measurements of model mechanical performance when inflated. Each symbol represents the mean of the mean values from three replicate models. Error bars represent 95% confidence intervals. A. Flexural stiffness (resistance to bending) of models plotted as a function of pressure inside the model. B. Isometric force exerted by the models plotted as a function of pressure inside the model. Positive values of isometric force indicate pushing along the end-to-end axis of the model, while negative values indicate pulling along that axis (Fig. 2D). C. Work done by models pushing along the end-to-end axis (Fig. 2E) plotted as a function of the load against which they were pushing. Work was calculated as described in Materials and Methods using the change in end-to-end distance as the models were inflated from an internal pressure of 28 kN/m² to an internal pressure of 41 kN/m².

DISCUSSION

Notochords as hydraulic or hydrostatic skeletons

Notochords are the axial skeleton of invertebrate chordates (cephalochordates, appendicularians, and tadpole larvae of ascidians), of agnathan fish, and of amphibian tadpoles. Notochords are the first axial skeletal structure to develop in the embryos of vertebrates, but they later become surrounded by cartilagenous or bony vertebrae in all but the agnathans (Kent and Miller, 1997). Not only do notochords perform mechanical work that helps reshape developing embryos (reviewed in Adams *et al.*, 1990; Koehl *et al.*, 1990), but they also play an important skeletal role in undulatory swimming. Long (1995) has examined the effects of notochord stiffness on undulatory swimming, and Symmons (1979) has discussed the importance of notochord elastic recoil in locomotion.

Many types of notochords appear to be hydrostatic or hydraulic systems composed of a fibrous sheath surrounding incompressible cells. Notochords in a variety of chordates have fibrous sheaths (*e.g.*, appendicularians, Olsson, 1964; Fennaux, 1998; lampreys, sturgeons, and lungfishes, Schmitz 1998; 1999; larval teleost fishes, Symmons 1979), and those fibers have been described as collagen (*e.g.*, cephalochordates, Flood 1975; hagfishes, Koob *et al.*, 1999; frog embryos, Adams *et al.* 1990; Koehl *et al.*, 1990; frog tadpoles, Bruns and Gross, 1970). Many notochords contain vacuolated cells (ascidian tadpoles, Cloney 1969; cephalochordates, Flood, 1975; lampreys, sturgeons, and lungfishes, Schmitz, 1998, 1999; hagfishes, Koob *et al.*, 1999; larval trout, Symmons, 1979; frog embryos, Adams *et al.*, 1990; Koehl *et al.*, 1990; frog tadpoles, Bruns and Gross, 1970), and some also contain extracellular fluid-filled spaces (*e.g.*, appendicularians, Olsson, 1964; Fennaux, 1998; ascidian tadpoles, Cloney, 1969). The notochord cells in cephalochordates also contain transverse paramyosin muscle fibers (*e.g.*, Guthrie and Banks, 1970; Flood, 1975). The notochord is pressurized (cephalochordates, Guthrie and Banks, 1970; Flood, 1975; sturgeons, Long,

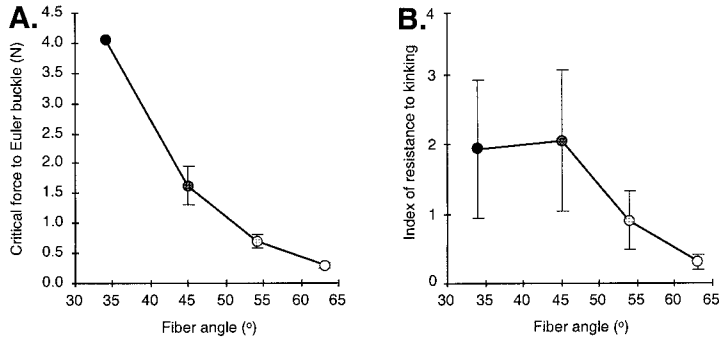


FIG. 8. Indices of the relative resistance of models to buckling when inflated to an internal pressure of 55 kN/m², plotted as a function of fiber angle when uninflated. Error bars represent 95% confidence intervals. Calculation of these indices is described in Materials and Methods. A. The critical force to Euler buckle is an index of the resistance to elastic bowing of a column bearing a compressive load. Each symbol represents the mean of the mean values from three replicate models. B. The index of resistance to kinking is a measure of the relative resistance to undergoing local buckling of a hollow, pressurized column or beam subjected to a bending load. Each symbol represents the mean of the values calculated for each of the three replicate models.

1995), and that internal pressure is produced osmotically (*e.g.*, appendicularians, Fennaux, 1998; hagfishes, Koob *et al.*, 1994, 1999; frog embryos, Adams *et al.*, 1990; Koehl *et al.*, 1990). The flexural stiffness of a notochord is increased when it is osmotically inflated (Adams *et al.*, 1990; Koehl *et al.*, 1990; Koob *et al.*, 1999), and the internal pressure is increased when a notochord is bent (Long, 1995).

The general principles revealed by our study of how fiber angle affects the mechanical performance of inflating hydraulic skeletons should apply not only to notochords of *X. laevis* embryos, but also to other types of fiber-reinforced, osmotically-pressurized notochords, as well as to inflating hydraulic skeletons of invertebrates and plants.

Design of hydraulic skeletons

Curved hydraulic cylinders (such as the notochords of early tail-bud embryos of frogs) whose walls are reinforced with nearly inextensible fibers in a crossed-helical arrangement (such as the collagen fibers in notochord sheaths) straighten and stiffen when they are inflated, regardless of the orientation of the reinforcing fibers. The mechanism responsible for this straightening is explained in Figure 9.

Only those cylinders reinforced with fibers at high angles ($\theta \geq 54^\circ$) increase the distance between their front and back ends

when they straighten upon inflation. As their internal pressure is increased, straightening cylinders with high θ 's push with greater force and do more work against a given compressive load than do cylinders with low θ 's, but they are also more susceptible to bowing and kinking. In contrast, cylinders with low θ 's are stiffer when inflated, and thus they are more resistant to being bent (*e.g.*, by lateral muscle contraction), and they can sustain larger compressive loads on their ends without buckling.

A θ near 54° appears to be a "good" design for a structure like the embryonic notochord that pushes against a load when it inflates; this θ represents a compromise between the ability to elongate and push versus the ability to resist buckling. A curved hydraulic cylinder reinforced with fibers at 54° can straighten and push when inflated, but is stiffer and more resistant to buckling than those with higher θ 's. Nonetheless, the θ of 54° of embryonic frog notochords may simply be the passive physical result of their osmotic inflation (because the maximum volume that can be contained in a cylinder reinforced with inextensible fibers occurs when θ is $54^\circ 44'$).

Certain designs of hydraulic and hydrostatic skeletons permit rapid elongation. Constant-volume cylindrical hydrostatic skeletons can change shape and exert forces on the environment via the action of antagonistic circumferential muscles (whose con-

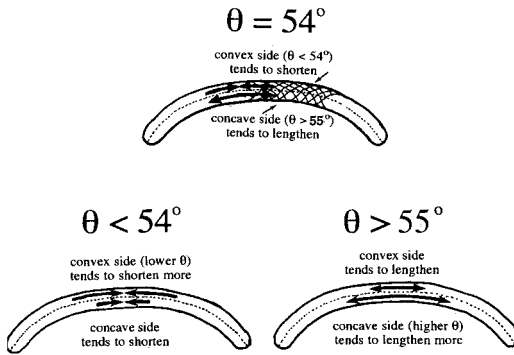


FIG. 9. Mechanism of straightening in notochord models. Continuous inextensible fibers wrap around the circumference of a curved model at an average fiber angle (θ) relative to the axis (dashed line) of the cylinder. However, because the convex side of the curved model is longer than the concave side, the θ of the fibers as they wrap around the convex side has to be lower than their θ as they wrap around the concave side. For a model with fibers at a mean θ of 54° , the θ of fibers on the convex side is slightly greater than $54^\circ 44'$, so that side tends to shorten when inflated, while the θ of the fibers on the concave side of the model is slightly less than $54^\circ 44'$, hence that side tends to elongate when inflated. The net result of the concave side lengthening and the convex side shortening is straightening of the model. For a model with mean $\theta < 54^\circ$, both sides shorten when inflated, but the convex side (which has a lower θ than the concave side) can shorten more before its θ reaches $54^\circ 44'$ than can the concave side. Similarly, for a model with mean $\theta > 55^\circ$, both sides lengthen when inflated, but the concave side (which has a higher θ than the convex side) lengthens more before its θ reaches $54^\circ 44'$ than can the convex side. Therefore, regardless of the initial mean θ of a curved model, the difference in the θ of fibers on the convex and concave sides of the model leads to the straightening of the model when inflated.

traction makes the hydrostat long and slender) and longitudinal muscles (whose contraction makes the cylinder sort and wide, or bends the cylinder) in the walls of the cylinders (*e.g.*, Chapman 1958, 1975; Clark, 1964; Wainwright, 1988). Variable-volume hydraulic cylinders, which are inflated by the contraction of muscles elsewhere in the body or are pumped up osmotically, can change shape not only by the action of muscles in their walls, but also by inflation and deflation. In hydrostatic systems of constant volume, long, slender cylinders have a greater rate of elongation for a given rate of contraction of circumferential muscles than do short, wide cylinders (Kier and Smith, 1985). In inflating hydrau-

lic systems, cylinders reinforced with fibers at high θ have a greater rate of lengthening for a given rate of volume increase than do cylinders with low θ 's, but are easily bent and buckled when they become long and slender upon inflation. Thus, high θ 's represent an effective design for hydraulic structures such as food-capturing tentacles that should elongate rapidly but that do not bear large compressive or bending loads.

Hydraulic cylinders reinforced with fibers at low θ 's shorten and pull when inflated, thereby providing an alternative mechanism to contraction of longitudinal muscles by which organisms can pull. Indeed, man-made McKibben artificial muscles are actuators that shorten when pneumatically inflated because they are reinforced with fibers at low θ (*e.g.*, Chou and Hannaford, 1996).

ACKNOWLEDGMENTS

This research was supported by NSF grant #IBN-9220525 to R. Keller and M. Koehl, and by a MacArthur Foundation Fellowship to M. Koehl. We are grateful to S. Wainwright for the use of facilities at the Biodesign Studio, Duke University, for fabrication of our models. We thank R. Kwak and M. Reyes for technical assistance, and R. Keller, W. Keir, M. McHenry, and S. Wainwright for helpful discussions.

REFERENCES

- Adams, D. S., R. E. Keller, and M. A. R. Koehl. 1990. Mechanism of straightening and elongation of the notochord of *Xenopus laevis*. *Development* 110: 115–130.
- Alexander, R. M. 1983. *Animal mechanics*. 2nd ed. Blackwell Scientific Publications, Oxford.
- Alexander, R. M. 1987. Bending of cylindrical animals with helical fibres in their skin or cuticle. *J. Theor. Biol.* 124:97–110.
- Bruns, R. and J. Gross. 1970. Studies on the tadpole tail: Structure and organization of the notochord and its covering layers in *Rana catesbeiana*. *Am. J. Anat.* 128:193–224.
- Chapman, G. 1958. The hydrostatic skeleton in the invertebrates. *Biol. Rev.* 33:338–371.
- Chapman, G. 1975. Versatility of hydraulic systems. *J. Exp. Zool.* 194:249–270.
- Chou, C.-P. and B. Hannaford. 1996. Measurement and modeling of McKibben pneumatic artificial muscles. *IEEE Transactions on Robotics and Automation* 12:90–102.

- Clark, R. B. 1964. *Dynamics of metazoan evolution*. Clarendon Press, Oxford.
- Clark, R. B. and J. B. Cowey. 1958. Factors controlling the change of shape of certain Nemertean and Turbellarian worms. *J. Exp. Biol.* 35:731–748.
- Cloney, R. A. 1964. Cytoplasmic filaments and morphogenesis: The role of the notochord in ascidian metamorphosis. *Z. Zellforsch. Mikrosk. Anat.* 100:31–53.
- Cosgrove, D. J. 1987. Mechanical and hydraulic aspects of plant cell growth. In J. Bereiter-Hahn, O. R. Anderson, and W.-E. Reif (eds.), *Cytomechanics*, pp. 215–229. Springer-Verlag, Berlin.
- Fenaux, R. 1998. Anatomy and functional morphology of the Appendicularia. In Q. Bone (ed.), *The biology of pelagic tunicates*, pp. 25–34. Oxford University Press, New York.
- Flood, P. R. 1975. Fine structure of the notochord of amphioxus. *Symp. Zool. Soc. Lond.* 36:81–104.
- Gilbert, S. F. 1985. *Developmental biology*. Sinauer Associates, Inc., Sunderland, Massachusetts.
- Green, P. 1980. Organogenesis—A biophysical view. *Ann. Rev. Plant Physiol.* 31:51–82.
- Guthrie, D. M. and J. R. Banks. 1970. Observations on the junction and physiological properties of a fast paramyosin muscle: The notochord of amphioxus. *J. Exp. Biol.* 52:125–138.
- Hettiaratchi, D. R. P. and J. R. O'Callaghan. 1978. Structural mechanics of plant cells. *J. Theor. Biol.* 74:235–257.
- Kelly, D. A. 1997. Axial orthogonal fiber reinforcement in the penis of the Nine-banded Armadillo (*Dasyurus novemcinctus*). *J. Morphol.* 233:249–255.
- Kelly, D. A. 1999. Expansion of the tunica albuginea during penile inflation in the nine-banded armadillo (*Dasyurus novemcinctus*). *J. Exp. Biol.* 202: 253–265.
- Kent, G. C. and L. Miller. 1997. *Comparative anatomy of the vertebrates*. 8th ed. William C. Brown, Publishers, Dubuque, Iowa.
- Kier, W. M. and K. K. Smith. 1985. Tongues, tentacles, and trunks: The biomechanics of movement in muscular hydrostats. *J. Zool. Linn. Soc.* 83:307–324.
- Koehl, M. A. R. 1990. Biomechanical approaches to morphogenesis. *Seminars in Developmental Biology* 1:367–378.
- Koehl, M. A. R., D. S. Adams, and R. E. Keller. 1990. Mechanical development of the notochord in early tail-bud amphibian embryos. In N. Akkas (ed.), *Biomechanics of active movement and deformation of cells*, pp. 471–485. Springer-Verlag, Berlin.
- Koob, T. J., J. T. Kielstein, L. Koob-Emunds, and H. Stolte. 1994. Physicochemical properties and proteoglycans of hagfish (*Myxine glutinosa*) notochord. *Bulletin MDIBL.* 33:5–8.
- Koob, T. J., J. A. Trotter, and J. H. Long. 1999. Notochord function in hagfish: How structure and composition impact bending properties. *Amer. Zool.* 38:146A.
- Long, J. H. J. 1995. Morphology, mechanics, and locomotion: The relation between the notochord and swimming motions in sturgeon. *Env. Biol. Fishes.* 44:199–211.
- Moore, S. W., R. E. Keller, and M. A. R. Koehl. 1995. The dorsal marginal stiffens anisotropically during its convergent extension in the gastrula of *Xenopus laevis*. *Development* 121:3131–3140.
- Murphy, J. S. 1990. *The condom industry in the United States*. McFarland & Company, Inc., Jefferson, North Carolina.
- Olsson, R. 1964. Comparative morphology and physiology of the Oikopleura notochord. *Isreal J. Zool.* 14:213–220.
- Quillin, K. J. 1998. Ontogenetic scaling of hydrostatic skeletons: Geometric, static stress and dynamic stress scaling of the earthworm *Lumbricus terrestris*. *J. Exp. Biol.* 201:1871–1883.
- Schmitz, R. J. 1998. Comparative ultrastructure of the cellular components of the unconstricted notochord in the sturgeon and the lungfish. *J. Morphol.* 236:75–104.
- Schmitz, R. J. 1999. Implications of notochord ultrastructure on the function and evolution of the vertebrate axial skeleton. *Am. Zool.* 38:146A.
- Sherrer, R. E. 1967. Filament wound cylinders with axial-symmetric loads. *Journal of Composite Materials* 1:344–355.
- Skierczynski, B. A., R. J. A. Wilson, W. B. J. Kristan, and R. Skalak. 1996. A model of the hydrostatic skeleton of the leech. *J. Theor. Biol.* 181:329–342.
- Swanson, C. J. 1974. Application of thin shell theory to helically-wound fibrous cuticles. *J. Theor. Biol.* 43:293–304.
- Symmons, S. 1979. Notochordal and elastic components of the axial skeleton of fishes and their functions in locomotion. *J. Zool., Lond.* 189:157–206.
- Tondu, B., and P. Lopez. 1995. Theory of an artificial pneumatic muscle and application to the modelling of McKibben artificial muscle. *Comptes Rendus De L'Academie Des Sciences Serie II* 320: 105–114.
- Wadepuhl, M. and W.-J. Beyn. 1989. Computer simulation of the hydrostatic skeleton. The physical equivalent, mathematics and application to worm-like forms. *J. Theor. Biol.* 136:379–402.
- Wainwright, S. A., W. D. Biggs, J. D. Currey, and J. W. Gosline. 1976. *Mechanical design in organisms*. Princeton University Press, Princeton.
- Wainwright, S. A. 1988. *Axis and circumference*. Harvard University Press, Cambridge, Massachusetts.
- Woodley, J. D. 1967. Problems in the ophiuroid water-vascular system. *Symp. Zool. Soc. Lond.* 20:75–104.
- Woodley, J. D. 1980. The biomechanics of Ophiuroid tube-feet. In M. Jangoux (ed.), *Echinoderms: Present and past*, pp. 293–299. A.A. Balkema, Rotterdam.